Translational Oncology 13 (2020) 100752

Contents lists available at ScienceDirect

Translational Oncology

journal homepage: www.elsevier.com/locate/tranon

The Elusive Link Between Cancer FDG Uptake and Glycolytic Flux Explains the Preserved Diagnostic Accuracy of PET/CT in Diabetes

Vanessa Cossu [1,2], Matteo Bauckneht [1,2], Silvia Bruno [3], Anna Maria Orengo [1], Laura Emionite [4], Enrica Balza [5], Patrizia Castellani [5], Patrizia Piccioli [5], Alberto Miceli [2], Stefano Raffa [2], Anna Borra [2], Maria Isabella Donegani [2], Sebastiano Carlone [5], Silvia Morbelli [1], Silvia Ravera [3], Gianmario Sambuceti [1,2], Cecilia Marini [1,6,*]

[1] Nuclear Medicine, IRCCS Ospedale Policlinico San Martino, Genova, Italy
[2] Department of Health Sciences, University of Genoa, Italy
[3] Department Experimental Medicine, University of Genoa, Italy
[4] Animal Facility, IRCCS Ospedale Policlinico San Martino, Genoa, Italy
[5] Cell Biology Unit, IRCCS Ospedale Policlinico San Martino, Genoa, Italy
[6] CNR Institute of Molecular Bioimaging and Physiology (IBFM), Milan, Italy

ARTICLE INFO

Article history:
Received 4 January 2020
Received in revised form 5 February 2020
Accepted 26 February 2020
Available online xxxx

ABSTRACT

This study aims to verify in experimental models of hyperglycemia induced by streptozotocin (STZ-DM) to what degree the high competition between unlabeled glucose and metformin (MET) treatment might affect the accuracy of cancer FDG imaging. The study included 36 "control" and 36 "STZ-DM" Balb/c mice, undergoing intraperitoneal injection of saline or streptozotocin, respectively. Two-weeks later, mice were subcutaneously implanted with breast (4 T1) or colon (CT26) cancer cells and subdivided in three subgroups for treatment with water or with MET at 10 or 750 mg/Kg/day. Two weeks after, mice were submitted to micro-PET imaging. Enzymatic pathways and response to oxidative stress were evaluated in harvested tumors. Finally, competition by glucose, 2-deoxyglucose (2DG) and the fluorescent analog 2-[N-(7-nitrobenz-2-oxa-1,3-diazol-4-yl)amino]-2-deoxyglucose (2-NBDG) on FDG uptake was studied in 4 T1 and CT26 cultured cells. STZ-DM slightly decreased cancer volume and FDG uptake rate (MRF). More importantly, it also abolished MET capability to decelerate lesion growth and MRF. This metabolic reprogramming closely agreed with the activity of hexose-6-phosphate dehydrogenase within the endoplasmic reticulum. Finally, co-incubation with 2DG virtually abolished FDG and 2-NBDG uptake within the endoplasmic reticulum in cultured cells. These data challenge the current dogma linking FDG uptake to glycolytic flux and introduce a new model to explain the relation between glucose analogue uptake and hexoses reticular metabolism. This selective fate of FDG contributes to the preserved sensitivity of PET imaging in oncology even in chronic moderate hyperglycemic conditions.

Background

The wide clinical utilization of cancer imaging with [^{18}F]-2-deoxy-glucose (FDG) largely exploits the link between disease aggressiveness and activation of the so-called Warburg effect, i.e. the high glycolysis rate regardless oxygen availability [1–10]. FDG kinetic features are well suited to highlight this metabolic reprogramming [11–14]. This tracer shares with glucose both trans-membrane transport and subsequent phosphorylation by hexokinases (HKs); however, the produced FDG-6-phoshate (FGD6P) accumulates within the cytosol as a terminal metabolite not accessible by downstream enzymes. Thus, normalizing late tracer retention for its technical determinants (injected dose and body weight) provides the "standardized uptake value" (SUV) that so far is interpreted as a clinically accessible index of cancer glycolytic flux [15].

Despite its almost general acceptance, the direct link between FDG accumulation and glycolysis rate is profoundly challenged in the daily clinical practice with hyperglycemic patients. The direct competition by unlabeled glucose and the consequent decrease in tracer uptake should imply to normalize cancer SUV for glycaemia. Nevertheless, this procedure has been shown not to provide any clinical benefit and even to impair measurement reproducibility [16]. Moreover, cancer SUV has been found to be independent of serum glucose level in >8000 patients with glycemia ≤200 mg/dl [17]. Consequently, current guidelines do not propose any SUV normalization, while they indicate the feasibility of FDG imaging in diabetic patients even in the presence of serum glucose levels as high as 200 mg/dl [7].

According to these "epidemiological" observations, the limited relevance of moderate hyperglycemia on tracer retention suggests a relatively loose link between FDG uptake and glucose consumption in cancer. This

* Address all correspondence to: Cecilia Marini, c/o Nuclear Medicine, IRCCS Ospedale Policlinico San Martino, Genova, Italy.
E-mail address: cecilia.Marini@unige.it. (C. Marini).

http://dx.doi.org/10.1016/j.tranon.2020.100752

concept agrees with the magnetic spectrometric evidence that more than 50% of adsorbed FDG is retained in the cell as metabolites downstream FDG6P [18–20]. Similarly, FDG uptake in brain [21], myocardium [22], skeletal muscle [23] and cancer [24] has been found to be largely independent of glycolytic flux and strictly dependent upon the activity of hexose-6-phosphate dehydrogenase (H6PD) [21–24]. This autosomic counterpart of the cytosolic glucose-6-phosphate-dehydrogenase (G6PD) is confined within the endoplasmic reticulum (ER) where it can oxidize several hexoses (including FDG, FDG6P, 2DG and 2DG6P) to trigger a specific ER pentose-phosphate pathway (PPP) [25,26]. As a relevant feature, the catalytic function of this omnivore enzyme is impaired by metformin (MET) that markedly reduces FDG uptake while simultaneously accelerating glycolytic flux in experimental cancers [27–36]. This drug action might thus further hamper PET/CT sensitivity in the large population of type-2 diabetes mellitus (DM) patients submitted to this technique under MET treatment.

The present study thus aimed to verify in experimental models of sustained hyperglycemia induced by streptozotocin (STZ-DM) to what degree the high competition between unlabeled glucose and MET treatment might affect the accuracy of cancer FDG imaging.

Material and Methods

Chemicals

For chemicals see Supplementary Materials.

Cell Lines and Animal Models

Murine syngeneic cell-lines of colon-rectal (CT26) and breast cancer (4 T1) were purchased from ATCC (LGC Standards Srl, Milan, Italy) and cultured as previously described [24,27]. All animal experiments were performed in accordance with guidelines and regulations (Italian 26/2014 and EU 2010/63/UE directives) and were approved by the local Ethical Committee and Italian Ministry of Health. The study included 72 six-weeks-old male BALB/c mice (Charles River, Italy); 36 "STZ-DM" animals received intraperitoneal STZ (150 mg), the remaining received only saline (controls). Two weeks thereafter, oral glucose tolerance test (OGTT) was performed administering a glucose load (1 g/Kg) and assaying serum glucose level at 15, 30, 60 and 120 minutes. The day after, both controls and STZ-DM cohorts were divided into two groups (n = 18) that were subcutaneously inoculated in dorsal hip with $5x10^5$ CT26 or 4 T1 cells, respectively. Each cluster was further subdivided into three subgroups (n = 6) that were untreated or treated with MET diluted in drinking water as to administer a daily dose of 10 (MET-10) or 750 mg/kg (MET-750), respectively. Treatment was continued for 2 weeks up to the day of micro-PET imaging. D.

Experimental Micro-PET Imaging

Fourteen days after cells inoculation, mice were fasted for 6 hours and weighted to be anesthetized with intra-peritoneal ketamine (100 mg/kg) (Imalgere, Milan, Italy) and xylazine (10 mg/kg) (Bio98, Italy). Cancer volume was determined by using external caliper and tumor volume was calculated using the following equation:

$$\text{tumor volume } (\mu l) = (\text{length} \times \text{width} \times \text{thickness}) \times \frac{\pi}{6.}$$

expressing length, width and thickness in mm [27]. Serum glucose level was tested, and animals were positioned in a dedicated micro-PET system (Albira, Bruker, USA). FDG (3-4 MBq) was injected through a tail vein, soon after start of a 40 minutes list-mode acquisition. Mice were euthanized by cervical dislocation, tumors were harvested and submitted to either immunohistochemical or biochemical analysis, (n = 3 per group).

Image Processing

According to our procedure [21–24], acquisition was binned in the following frames: 10 × 15 s, 5 × 30 s, 2 × 150 s, 6 × 300 s, 1 × 600 s; images were reconstructed using maximal likelihood expectation maximization method (MLEM). An experienced observer identified a volume of interest (VOI) in the left ventricle to plot the arterial input function that served for FDG clearance calculation [21–24]. Parametric maps of FDG accumulation rate were thus obtained according to the Gjedde-Patlak graphical approach [37] and multiplied for serum glucose. A VOI was drawn on cancer lesion to estimate average FDG metabolic rate (MRF, in nmol × min^{-1} × g^{-1}). The same VOI was copied on the last frame to estimate SUV.

Ligand Tracer

In-vitro FDG uptake was evaluated using a dedicated instrument (LigandTracer white, Ridgeview, SE) according to our previously validated procedure [21–23,38]. 4 T1 and CT26 cell cultures were grown as previously described [24,27,38]. Soon before the experiment, culture medium was replaced with DMEM containing glucose at 5.5 mM or 11 mM and enriched with 1.8 to 2.2 MBq/ml FDG. Tracer uptake was measured by its disappearance from the medium over the 2 hours experiments. The same approach was used to estimate glucose consumption, with cells left in the medium for further 10 hours (Supplementary Materials). All experiments were performed in triplicate and data normalized for cell number. The effect of two MET concentrations (1 and 5 mM) was also tested.

The competition between FDG and 2DG was evaluated by measuring FDG uptake in cultures exposed to glucose-free DMEM enriched with 5.5 mM 2DG. This last evaluation was complemented by a further set of experiments in which the cell cultures were incubated for 2 hours with either glucose or 2DG, at the same 5.5 mM concentration, before their exposure to hexose-free DMEM enriched with FDG alone.

Spectrophotometric Assay

Three dedicated tumors of each group were homogenized in phosphate-buffer saline with a Potter-Elvehjem homogenizer and enzymatic assays were performed as described in Supplementary Materials [21–24].

Immunohistochemical Analysis

Immunohistochemical analysis is detailed in the Supplementary Materials.

Co-localization Experiments

Glucose co-localization with the ER was evaluated by confocal microscopy according to our validated protocol [21,23,24], described in the Supplementary Materials. Cells were incubated with glibenclamide and 2-[N-(7-nitrobenz-2-oxa-1,3-diazol-4-yl)amino]-2-deoxyglucose (2-NBDG) as indicator of ER and glucose-analogue accumulation site, respectively.

Statistical Analysis

The data are presented as mean ± standard deviation. Comparison between different groups was performed by analysis of variance (ANOVA) for multiple comparisons; Student *t* test, for paired or unpaired data, were used as appropriate. Statistical significance was considered at $P < .05$. Statistical analyses were performed using SPSS software 15.0 (Chicago, IL).

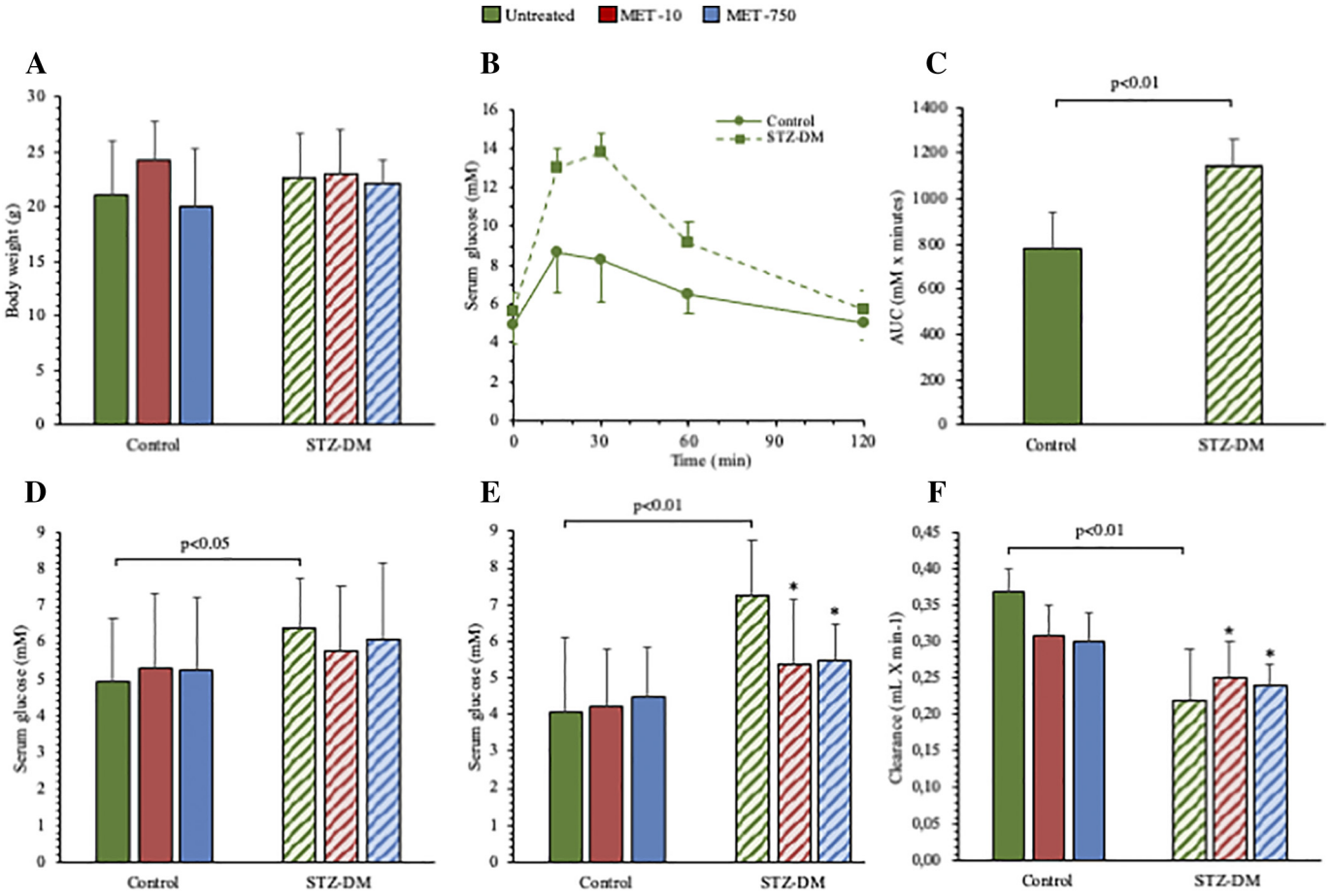

Figure 1. *Effect of STZ and MET on mice body weight, serum glucose level and clearance* Body weight in control (solid columns) and STZ-DM groups (dashed columns) of untreated (green) or low (red) or high dose (blue) MET-treated mice (Panel A, n = 12. Serum glucose levels after OGTT in the 36 control (solid line) and in the 36 STZ-DM mice (dashed line) (Panel B). Panel C shows the area under the curve, with solid and dashed columns reporting average values for control and STZ-DM mice, respectively. Fasting glycemia at cancer cells inoculation (Panel D): dashed columns indicate STZ-DM mice that have been treated with MET only after this measurement. Fasting glycemia at PET imaging (Panel E). Blood FDG clearance (Panel F) in control (solid columns) and STZ-DM mice (dashed columns) untreated (green) or under low (red) or high dose (blue) of MET. Data are expressed as mean ± SD (*$P < .05$ vs the corresponding control not treated by MET).

Results

Effect of Diabetes and Metformin Treatment on Serum Glucose Level

The studies were completed in all animals and no relevant side effects occurred after STZ or under MET treatments. Body weight was similar in all groups both at cells inoculation and at PET imaging (Figure 1*A*). At OGTT, the area under the curve was higher in STZ-DM mice than in controls (Figure 1, *B* and *C*). This difference persisted at the measurement of fasting glycaemia at cancer cells inoculation (Figure 1*D*). Two-weeks thereafter, soon before PET imaging, glucose level remained increased in untreated STZ-DM mice while it was lowered by both MET treatment regimens to values close to untreated controls (Figure 1*E*).

In STZ-DM mice, hyperglycemia was associated with a reduction in hexose uptake by whole body tissues as documented by the decrease in blood FDG clearance observed in diabetic mice, regardless the inoculated cell type (Figure 1*F*). As expected, MET antihyperglycemic action was not related to an enhanced insulin sensitivity since drug effect on tracer removal from the bloodstream was not appreciable in STZ-DM mice and was even decreased in a dose-dependent fashion in control ones.

Hyperglycemia and Metformin Effect on Cancer Growth and FDG Uptake

Anatomical volume of 4 T1 (Figure 2, *A* and *B*) and CT26 (Figure 2, *D* and *E*) cancers was superimposable in non-diabetic untreated mice and showed a similar dose-dependent reduction under both MET treatments (Figure 2, *B–E*). This evaluation also applied to the estimation of metabolically active lesion, since the volume of the manually drawn VOI on cancer lesion was remarkably similar and directly correlated with the anatomical estimation provided by caliper measurements (Suppl Figure 1). Drug effect on cancer growth nicely agreed with the corresponding response of MRF that was reduced by MET treatments in both 4 T1 (Figure 2*C*) and CT26 lesions (Figure 2*F*). These data thus extended our previous observations [20,23] indicating that MET decelerates cancer growth in normoglycemic mice.

STZ-DM decreased the growth of untreated 4 T1 cancers, while this effect did not reach the statistical significance for CT26 lesions (Figure 2, *B* and *E*). Again, this observation was at least partially reproduced by the estimated MRF that, despite the higher serum glucose level, was slightly lower in cancers hosted by hyperglycemic animals with respect to control ones (Figure 2, *A*, *C–D* and *F*).

STZ-DM also affected cancer response to MET, whose capability to decelerate lesion growth was either reverted to an increase in 4 T1 models (Figure 2, *A* and *B*) or abolished in CT26 tumors (Figure 2, *D* and *E*). Again, FDG uptake kinetics matched this response, since MET slightly increased MRF in STZ-DM 4 T1 cancers (Figure 2, *A* and *C*) while being virtually ineffective in STZ-DM CT26 ones (Figure 2, *D* and *F*).

Differently from MRF, the conventional analysis of cancer FDG uptake was not affected by either STZ-DM or MET. In fact, the deceleration in FDG clearance and the consequent prolongation of blood tracer availability

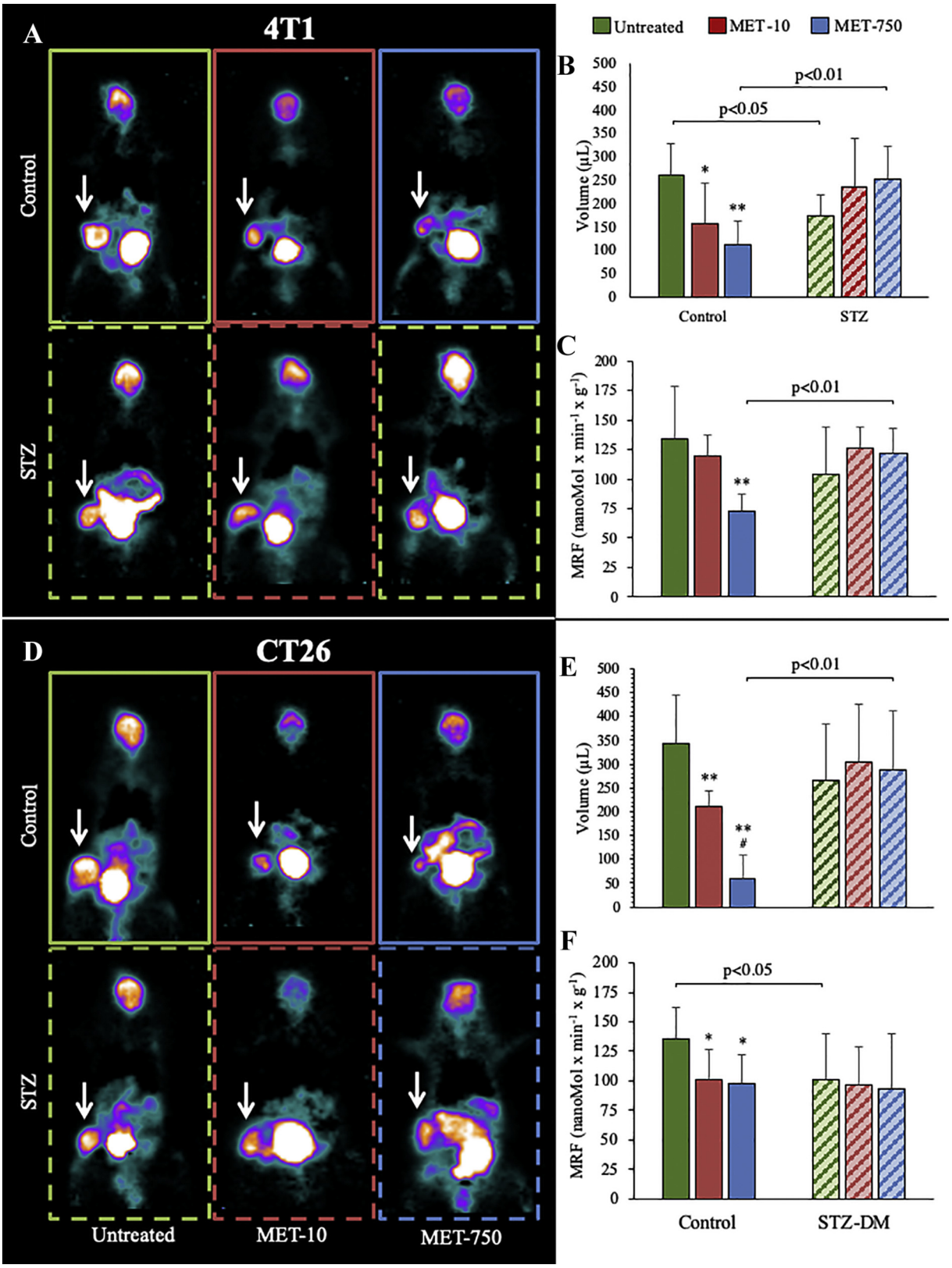

Figure 2. In vivo *effects of STZ-DM and metformin on cancer growth and MRF.* Parametric maps of representative mice untreated (green), under low (red) or high (blue) MET doses, 2 weeks after 4 T1 (Panel A) or CT26 (Panel D) cell implantation. White arrows indicate the tumors. Tumor volumes are expressed in Panels B (4 T1) and E (CT26); cancer metabolic rate of FDG uptake are represented in Panels C (4 T1) and F (CT26), respectively. Data are expressed as mean ± SD, n = 6 for each group; *$P < .05$, ** $P < .01$ vs the corresponding control not treated by MET, # $P < .05$ vs MET-10).

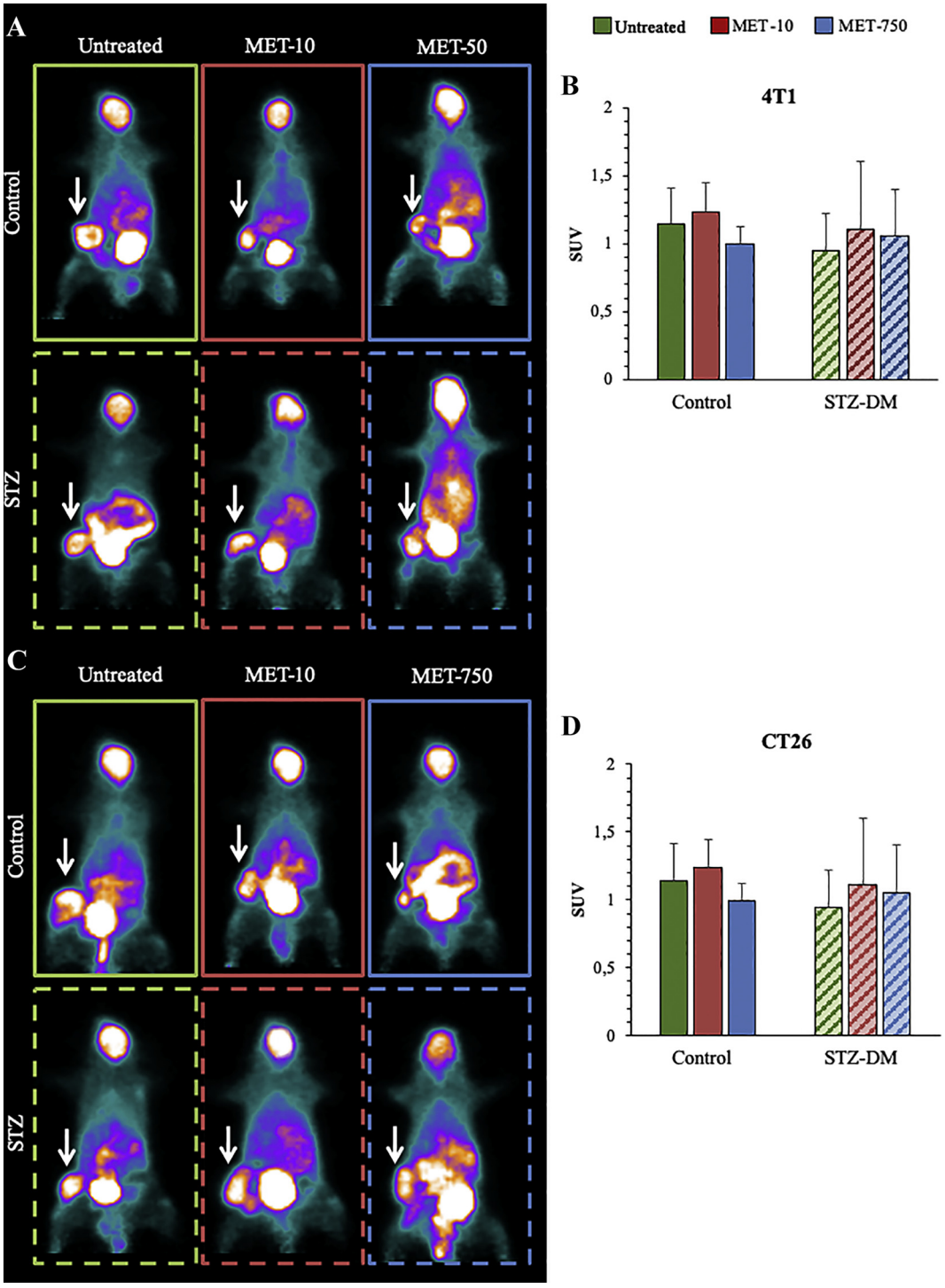

Figure 3. In vivo *effects of STZ-DM and metformin on cancer Standardize Uptake Value* Cancer SUV of representative mice untreated (green) or under low (red) or high (blue) MET doses, 2 weeks after implantation of 4 T1 (Panel A) or CT26 (Panel C) cells. Cancer average SUV (white arrows) is expressed in Panels B and D for 4 T1 and CT26, respectively. Data are expressed as mean ± SD (n = 6; $^{*}P < .05$; $^{**}P < .01$ vs the corresponding control not treated by MET).

preserved similar cancer SUVs in all subgroups (Figure 3, *A* and *B* for 4 T1; Figure 3, *C* and *D* for CT26).

Effect of Diabetes and Metformin on Enzymatic Pathway in 4 T1 and CT26 Cancers

To evaluate the determinants of FDG uptake, we analyzed the key enzymatic activities of glucose metabolism in harvested tumors, as to consider the contribution of all cells populating the lesion representative of both cancer and surrounding microenvironment. In 4 T1 cancers, both STZ-DM and MET treatment increased HK and PFK activity (Figure 4, *A* and *C*). CT26 lesions showed a less evident response to STZ-DM that, however, flattened the response of these enzymes to MET (Figure 4, *B* and *D*). A similar observation applied to G6PD (Suppl Figure 2): its activity was scarcely (in 4 T1) or not (in CT26) modified by MET in cancers hosted by non-diabetic animals. By contrast, it was enhanced by the biguanide only in lesions grown in 4 T1

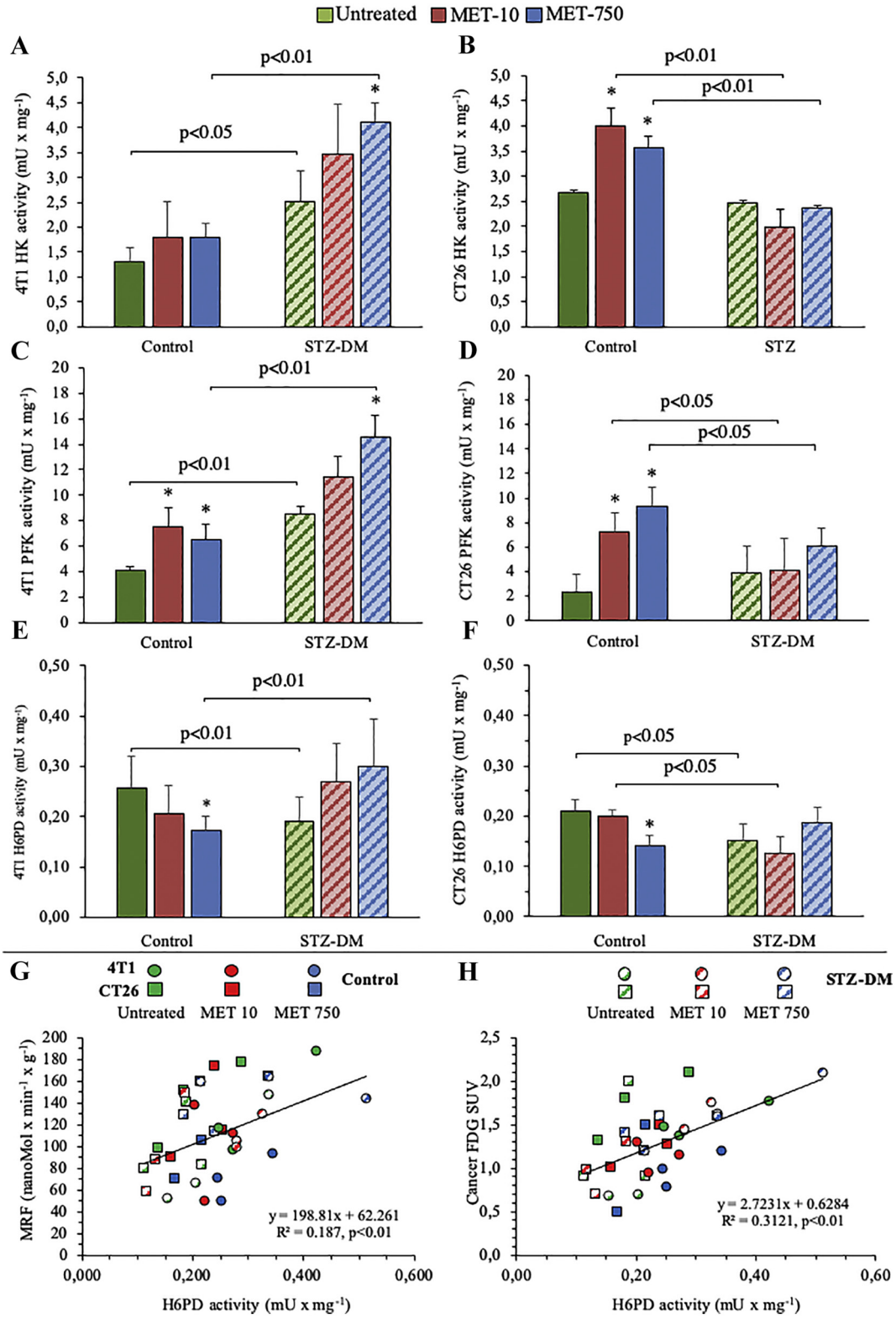

Figure 4. *Effects of MET and STZ on the main regulators of glucose metabolism.* Catalytic activities of HK (Panels A, B), PFK (Panels C, D) and H6PD (Panels E, F) in 4 T1 (left) and CT26 (right) cancers, in untreated groups (solid columns) and STZ-DM groups (striped columns). Data are expressed as mean ± SD (n = 3; *$P < .05$; **$P < .01$ vs the corresponding control not treated by MET). Correlation between MRF-H6PD activity (Panel G) and FDG SUV-H6PD activity (Panel H) in 4 T1 (circles, n = 18) and CT26 (squares, n = 18) tumors harvested from either control (solid signs) or STZ-DM (dashed signs) mice; according to the conventional scheme, MET treatment is reported as green (absent), red (low) or blue (high) dose.

hyperglycemic mice. Thus, the activity of enzymes catalyzing the rate-limiting steps of either glycolysis or cytosolic PPP could not explain the reduction in estimated MRF induced by either STZ-DM or MET (Figure 2, *C* and *F*).

We thus moved our attention to H6PD. Actually, STZ-DM inhibited the catalytic function of this reticular enzyme in both cancer models (Figure 4, *E* and *F*). Moreover, H6PD activity was reduced by high dose of MET in

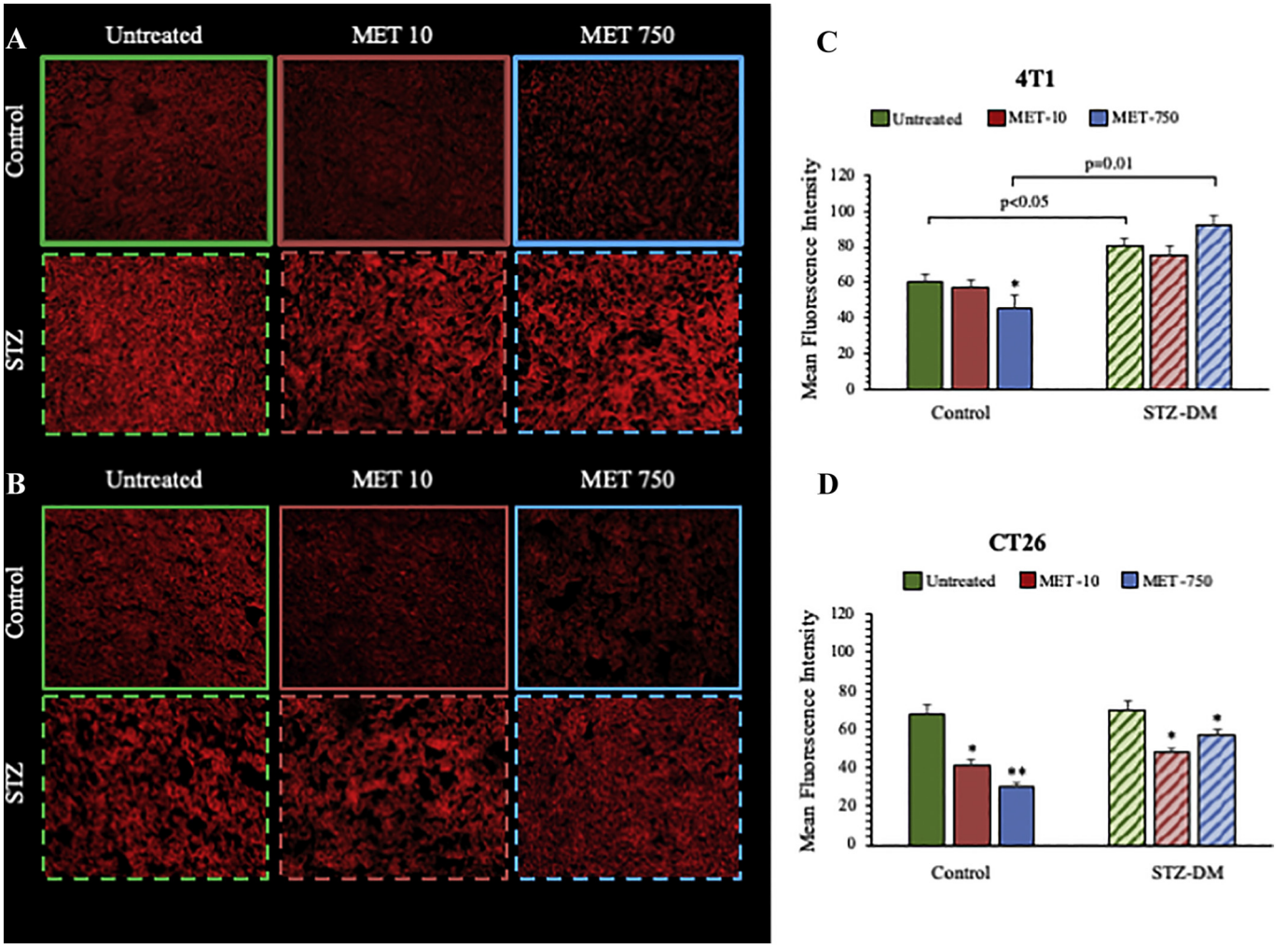

Figure 5. *Mercury orange as a fluorogenic probe for measuring anti-oxidant response.* Representative images of MO intensity in untreated (green) or under low (red) or high MET doses (blue) in 4 T1 (Panel A) and CT26 (Panel B) cancers harvested from control and STZ-DM mice. Average MO intensities are expressed in Panels C and D for 4 T1 and CT26, respectively. Data are expressed as mean ± SD (n = 3; *$P < .05$ vs the corresponding control not treated by MET).

cancers harvested from non-diabetic mice while it was virtually not affected by the biguanide in STZ-DM lesions. Thus, H6PD activity mimicked the behavior of MRF. This observation was strongly corroborated by the evidence of a direct, linear, relationship between H6PD enzymatic function and corresponding MRF in both 4 T1 and CT26 lesions regardless the experimental condition (Figure 4*G*). More importantly, this same correlation was observed when average cancer SUV was considered instead of MRF (Figure 4*H*).

Overall, FDG uptake rates were not related to the presence or degree of inflammatory infiltrates: immunohistochemistry did not identify significant effects of either MET or STZ-DM on macrophage content (Suppl Figure 3); similarly, the cancer vascularization was unchanged by these treatments (Suppl Figure 4). By contrast, Mercury Orange (MO) staining showed a marked decrease in CT26 specimens hosted by non-diabetic mice treated with MET. This effect was less evident in tumors harvested from STZ-DM models (Figure 5). On the other hand, MET effect in 4 T1 lesions could be appreciated only in control mice treated with the highest drug dose (Figure 5).

Interference of MET and Glucose on In Vitro FDG Uptake

The direct competition between high levels of unlabeled glucose and FDG uptake in cancer cells was estimated in vitro by LigandTracer instrument. Doubling glucose concentration in the incubation medium from 5.5 to 11 mM (from 1 to 2 g/L) decreased by fourfold FDG uptake in both cultured 4 T1 and CT26 cells (Figure 6, *A* and *B*). Moreover, biguanide effect on FDG accumulation was markedly dependent upon glucose concentration in the medium: MET drastically *decreased* fractional tracer uptake in both cancer cells incubated with 5.5 mM glucose, while it was virtually ineffective at high glucose level (11 mM) (Figure 6, *A* and *B*). Intriguingly, this observation profoundly disagreed with the response of glucose consumption that showed a dose dependent *increase* to MET exposure regardless glucose availability in both cell types (Figure 6, *C* and *D*).

The elusive link between overall glucose consumption and FDG uptake was further corroborated by the large difference in FDG time-activity curves of cancer cells cultured in the presence of glucose or 2DG. Both cell lines showed a measurable FDG uptake in the presence of glucose 5.5 mM, while tracer accumulation was almost abolished by the incubation with 2DG at the same concentration (Figure 6, *E* and *F*). We thus verified whether this different response was a consequence of 2DG toxicity. To this purpose, cell cultures were incubated with either glucose or 2DG (5.5 mM) for 2 hours and thus moved into a hexose-free-medium enriched with FDG alone. Tracer uptake rate was even higher in cells previously exposed to the "false-metabolite" with respect to those cultured in the presence of glucose suggesting a preserved metabolic activity (Figure 6, *G* and *H*).

The divergent nature of competition provided by glucose and 2DG on FDG uptake was confirmed by imaging experiments using the 2DG analogue 2-NBDG. In the presence of glucose (5.5 mM), this fluorescence probe was preferentially accumulated within the ER identified by the

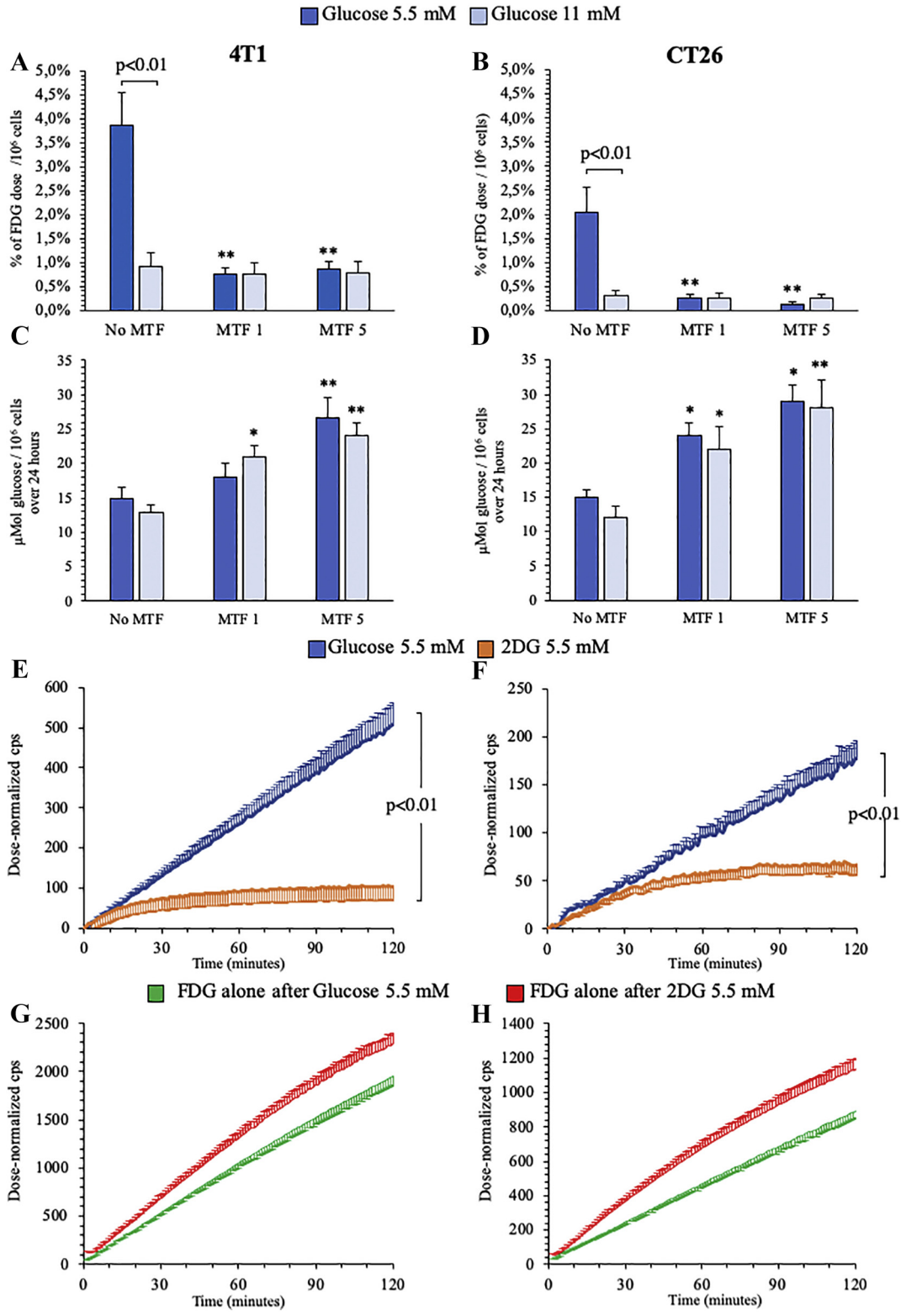

Figure 6. *Effect of different glucose and MET concentrations on 4 T1 and CT26 cells.* Fractional FDG uptake (Panels A-B) and glucose consumption (C-D) in presence of glucose 5 mM (blue) or 11 mM (light blue) under control, MET 1 mM and MET 5 mM treatments, in 4 T1 (left) and CT26 (right) cancer cells. FDG kinetic uptake in presence of glucose 5 mM (blue) or 2DG 5 mM (red) (Panels E-F) and FDG kinetic uptake in presence of FDG alone, after 2 h incubation of glucose 5 mM (blue) or 2DG 5 mM (red), in 4 T1 (left) and CT26 (right) cancer cells, respectively. Data are expressed as mean ± SD (n = 3; * = $P < .05$; ** = $P < .01$ vs the corresponding control not treated by MET).

glibenclamide staining (Figure 7, *A* and *B*). Incubation with the same 2DG concentration profoundly altered this intracellular compartmentalization and decreased the fraction of 2-NBDG containing voxels located within the ER (Figure 7, *A–C*).

Discussion

In the present experimental study, chronic moderate hyperglycemia did not significantly affect cancer FDG uptake, in agreement with current

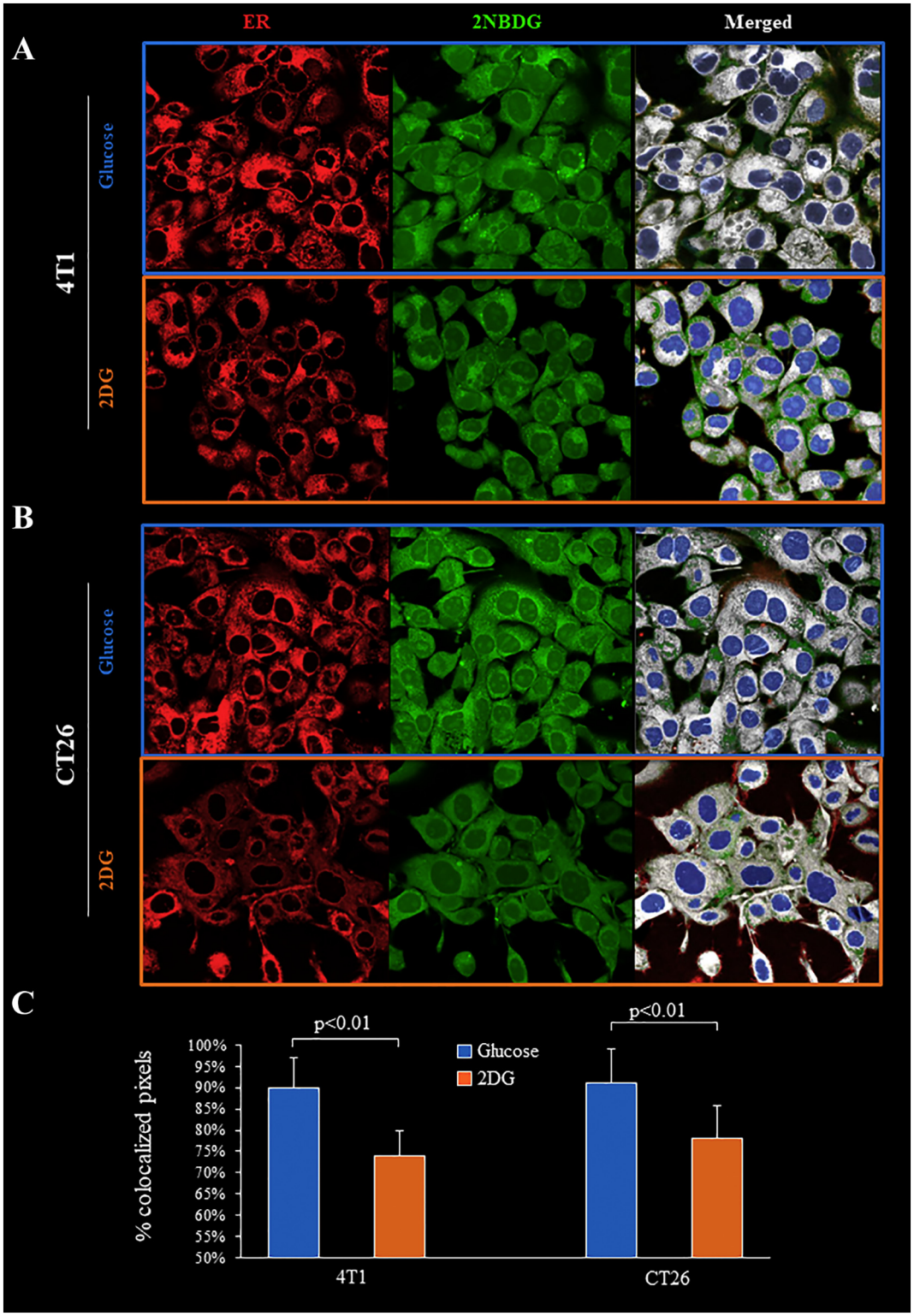

Figure 7. *Effect of incubation with 2DG on colocalization of 2-NBDG and ER signals* Confocal microscopy images of glibenclamide (ER, red), 2-NBDG (green), and merged (white) fluorescence in 4 T1 (Panel A) and CT26 (Panel B) cells incubated with glucose (light blue) or 2DG (orange). Nuclear staining (DAPI) is shown (blue). Panel C shows the % of colocalized pixels ± SD. (n = 3; * = $P < .05$; ** = $P < .01$ vs corresponding control).

guidelines that indicate metabolic PET/CT imaging in patients with fasting glucose levels up to 200 mg/dl [7]. This feature at least partially reflects the reduction in tracer sequestration by insulin-dependent normal tissues. Indeed, hyperglycemia was associated with a significant reduction in FDG clearance that protracted blood tracer availability, eventually preserving cancer SUV at the time of conventional image acquisition.

Besides this clinical confirmation, the present data also indicate a slightly reduced avidity for FDG in cancers grown in chronically hyperglycemic environment. This response is paralleled by a loss of sensitivity to MET, whose capability to simultaneously decrease FDG accumulation rate and growth was observed only in cancer hosted by control mice [24,27], while it was virtually absent in STZ-DM ones. This finding agrees with

previous studies showing that hyperglycemia inhibits MET capability to activate AMPK phosphorylation and thus prevents a main mechanism underlying biguanide antiproliferative effect [39,40]. The different behavior between normo- and hyperglycemic conditions and/or MET treatments was not explained by any impairment in the enzymes regulating cytosolic glucose degradation through glycolysis (HK and PFK) or PPP (G6PD). Actually, this observation seems to disagree with our previous studies [24,27]. Nevertheless, this divergence is only apparent since enzymatic activities were only evaluated in harvested cancers and, thus, in the absence of MET. As a consequence, the present data do not provide any insight about a possible direct drug interference on studied catalytic functions. By contrast, they confirm that MET effect on FDG uptake is relatively independent of cytosolic glucose metabolism in tumors hosted both by normoglycemic and hyperglycemic mice.

Effect of hyperglycemia and MET on cancer FDG retention was not significantly contaminated by host-derived cells recruited by inflammation or neo-angiogenesis. This finding was somewhat expected, since inflammation has been found to play a more relevant role in the preclinical/initial than in the late stage of cancer development [46] focus of our study. In agreement with this evidence, $CD206^+$ and $CD31^+$ infiltrates were scarcely represented in harvested tumors, regardless the exposure to STZ-DM or biguanide treatments.

More importantly, the metabolic response to increased glucose availability was reproduced in vitro. Indeed, doubling glucose concentration in the culture medium slowed by fourfold FDG accumulation rate and abolished the dose-dependent decrease in tracer uptake induced by MET. Intriguingly, both findings markedly disagreed with the response of glucose consumption, since “hyperglycemia” did not affect glucose removal from the incubation medium, nor it modified its dose-dependent increase in response to MET. Accordingly, hyperglycemia profoundly alters the relationship between glucose consumption and FDG uptake, i.e. the basis for interpreting cancer metabolic imaging. This consideration is corroborated by the response to 2DG, whose presence caused a markedly more pronounced reduction in FDG accumulation with respect to glucose at the same concentration. Since any possible toxicity was ruled out by the restoration of normal FDG uptake immediately after 2DG removal, the high competition between these two hexoses suggests that their common fate might be not shared by the ‘mother’ substance glucose.

Co-incubation with 2DG also impaired the ER compartmentalization of the fluorescent FDG analogue 2-NBDG confirming the role of this intracellular compartment as a preferential accumulation site of de-oxygenated glucose analogues [21–24,38]. In agreement with this concept, effect of both STZ-DM and MET on FDG uptake was at least partially reproduced by the behavior of H6PD, the trigger ER PPP [25,26], and by the direct linear relationship between the catalytic function of this enzyme and FDG uptake that was observed when all cancer types were considered regardless experimental group and MET treatment regimens.

The most acknowledged PPP function is the conversion of NADP to NADPH to support either bio-reductive syntheses of fatty acids and nucleic acids or antioxidant responses to redox stress. An increased generation of reactive oxidative species (ROS) in chronically hyperglycemic patients has been already reported [41,42]. The activation of glutathione dependent antioxidant responses documented by MO staining in 4 T1 lesions of STZ-DM tumors was actually paralleled by the behavior of G6PD function. Both responses were remarkably less evident in CT26 cancers. On the other hand, the responses of cancer H6PD activity and FDG uptake to STZ-DM were characterized by a matched slight decrease in both cancer types. Accordingly, the adherence between G6PD activity and MO staining suggests that hyperglycemia-related redox stress might preferentially trigger the antioxidant response within the cytosol through mechanisms that cannot be defined on the basis of the present study.

Several limitations of the present study need to be commented. Although several studies already used STZ to mimic type-2 diabetes [43–45], the observed hyperglycemia reflects the impaired insulin secretion, while the clinical model implies a simultaneous increase in serum levels of both glucose and insulin. Accordingly, further studies are needed to verify the adherence of the response observed in these experimental models to the clinical setting of diabetes mellitus. Similarly, the study only included male mice to avoid the resistance to streptozotocin usually observed in females [43–45]. Accordingly, the relative reduction in lesion volumes observed in hyperglycemic animals cannot be extended to indicate a decrease in cancer growth rate in diabetic patients.

Finally, the subcutaneous inoculation prevents an accurate description of the interference of hyperglycemia and MET on diagnostic accuracy of FDG imaging in colon-rectal cancer. Nevertheless, this procedure permitted us to characterize the response of CT26 lesions avoiding the confounding effect of high uptake by normal colonic enterocytes [35] exposed to the biguanide.

Supplementary data to this article can be found online at https://doi.org/10.1016/j.tranon.2020.100752.

Declarations

Ethics approval and consent to participate: All procedures involving animals were performed in respect of the current National and International regulations and were reviewed and approved by the Licensing and Animal Welfare Body of the Ospedale Policlinico San Martino, Genoa, Italy and by the Italian Ministry of Health, committee's reference number 832/2016-PR.

Consent for publication: All authors have agreed to publish this manuscript.

Availability of data and material: Data are available on reasonable request.

Competing interests: The authors declare that they have no competing interests.

Funding

This study was funded by the program “Ricerca Corrente,” line “Guest-Cancer Interactions,” by Compagnia di San Paolo (project ID Prot.: 2015.AAI4110.U4917) and by the grant AIRC “chemotherapy effect on cell energy metabolism and endoplasmic reticulum redox control” (IG 23201).

Authors' Contributions

Conception and design or analysis and interpretation of data, or both: CM, VC, GMS; Drafting of the manuscript or revising it critically for important intellectual content: VC, MB, CM, GMS; Animal experiments: LE, EB, PP, PC, AMO; in vitro experiments: VC, SB, SR, AMO, SC; Image analysis and image processing: MB, SC, SM, AB, AM, ID, SR; Statistic analysis of data: CM, VC, GMS; Final approval of the manuscript submitted: All authors

Acknowledgements

Not applicable.

References

[1] L.K. Shankar, J.M. Hoffman, S. Bacharach, et al., Consensus recommendations for the use of 18F-FDG PET as an indicator of therapeutic response in patients in national cancer institute trials, J Nucl Med 47 (2006) 1059–1066.
[2] A. Gallamini, C. Zwarthoed, A. Borra, Positron emission tomography (PET) in oncology, Cancers (Basel) 6 (2014) 1821–1889.
[3] D. Groheux, A. Cochet, O. Humbert, J.L. Alberini, E. Hindié, D. Mankoff, ^{18}F-FDG PET/CT for staging and restaging of breast cancer, J Nucl Med 57 (2016) 17S–26S.
[4] H. Jadvar, A. Alavi, S.S. Gambhir, 18F-FDG uptake in lung, breast, and colon cancers: molecular biology correlates and disease characterization, J Nucl Med 50 (2009) 1820–1827.
[5] M.E. Phelps, PET: the merging of biology and imaging into molecular imaging, J Nucl Med 41 (2000) 661–681.
[6] S.S. Gambhir, Molecular imaging of cancer with positron emission tomography, Nat Rev Cancer 2 (2002) 683–693.
[7] R. Boellaard, Standards for PET image acquisition and quantitative data analysis, J Nucl Med 50 (2009) 11S–20S.
[8] F. Fathinul, A.J. Nordin, W.F. Lau, 18[F]FDG-PET/CT is a useful molecular marker in evaluating tumour aggressiveness: a revised understanding of an in-vivo FDG-PET

imaging that alludes the alteration of cancer biology, Cell Biochem Biophys 66 (2013) 37–43.
[9] M.G. Vander Heiden, L.C. Cantley, C.B. Thompson, Understanding the Warburg effect: the metabolic requirements of cell proliferation, Science 324 (2009) 1029–1033.
[10] O. Warburg, ber den Stoffwechsel der Carcinomzelle, Naturwissenschaften 12 (1924) 1131–1137.
[11] O. Warburg, On the origin of cancer cells, Science 123 (1956) 309–314.
[12] P.P. Hsu, D.M. Sabatini, Cancer cell metabolism: Warburg and beyond, Cell 134 (2008) 703–707.
[13] L. Sokoloff, M. Reivich, C. Kennedy, et al., The [14C]deoxyglucose method for the measurement of local cerebral glucose utilization: theory, procedure, and normal values in the conscious and anesthetized albino rat, J Neurochem 28 (1977) 897–916.
[14] M. Reivich, D. Kuhl, A. Wolf, et al., The [18F]fluorodeoxyglucose method for the measurement of local cerebral glucose utilization in man, Circ Res 44 (1979) 127–137.
[15] M.A. Lodge, Repeatability of SUV in Oncologic 18F-FDG PET, J Nucl Med 58 (2017) 523–532.
[16] C. Sprinz, M. Zanon, S. Altmayer, et al., Effects of blood glucose level on 18F-fluorodeoxyglucose (18F-FDG) uptake for PET/CT in normal organs: an analysis on 5623 patients, Sci Rep 8 (2018) 2126.7.
[17] M. Eskian, A. Alavi, M. Khorasanizadeh, et al., Effect of blood glucose level on standardized uptake value (SUV) in 18F-FDG PET-scan: a systematic review and meta-analysis of 20,807 individual SUV measurements, Eur J Nucl Med Mol Imaging 46 (2019) 224–237.
[18] Y. Kanazawa, H. Yamane, S. Shinohara, S. Kuribayashi, Y. Momozono, Y. Yamato, et al., 2-Deoxy-2-fluoro-D-glucose as a functional probe for NMR: the unique metabolism beyond its 6-phosphate, J Neurochem 66 (1996) 2113–2120.
[19] G.A. Dienel, N.F. Cruz, Synthesis of deoxyglucose-1-phosphate, deoxyglucose1,6-biphosphate, and other metabolites of 2-deoxy-D-[^{14}C]glucose in rat brain in vivo: influence of time and tissue glucose level, J Neurochem 60 (1993) 2217–2231.
[20] R. Southworth, C.R. Parry, H.G. Parkes, R.A. Medina, P.B. Garlick, Tissue-specific differences in 2-fluoro-2-deoxyglucose metabolism beyond FDG-6-P : a 19 F NMR spectroscopy study in the rat, NMR Biomed 16 (8) (2003) 494–502.
[21] V. Cossu, C. Marini, P. Piccioli, et al., Obligatory role of endoplasmic reticulum in brain FDG uptake, Eur J Nucl Med Mol Imaging 46 (2019) 1184–1196.
[22] M. Bauckneht, F. Pastorino, P. Castellani, et al., Increased myocardial 18F-FDG uptake as a marker of doxorubicin-induced oxidative stress, J Nucl Cardiol (2019) https://doi.org/10.1007/s12350-019-01618-x.
[23] M. Bauckneht, V. Cossu, P. Castellani, et al., FDG uptake tracks the oxidative damage in diabetic skeletal muscle: An experimental study, Mol Metab 31 (2020) 98–108.
[24] C. Marini, S. Ravera, A. Buschiazzo, et al., Discovery of a novel glucose metabolism in cancer: The role of endoplasmic reticulum beyond glycolysis and pentose phosphate shunt, Sci Rep 6 (2016) 25092.
[25] G. Bánhegyi, A. Benedetti, R. Fulceri, S. Senesi, Cooperativity between 11beta-hydroxysteroid dehydrogenase type 1 and hexose-6-phosphate dehydrogenase in the lumen of the endoplasmic reticulum, J Biol Chem 279 (2004) 27017–27021.
[26] M. Csala, G. Bánhegyi, A. Benedetti, Endoplasmic reticulum: a metabolic compartment, FEBS Lett 580 (2006) 2160–2165.
[27] C. Marini, G. Bianchi, A. Buschiazzo, et al., Divergent targets of glycolysis and oxidative phosphorylation result in additive effects of metformin and starvation in colon and breast cancer, Sci Rep 6 (2016) 19569.
[28] A.K. Madiraju, D.M. Erion, Y. Rahimi, et al., Metformin suppresses gluconeogenesis by inhibiting mitochondrial glycerophosphate dehydrogenase, Nature 510 (2014) 542–546.
[29] G. Zhou, R. Myers, Y. Li, et al., Role of AMP-activated protein kinase in mechanism of metformin action, J Clin Invest 108 (2001 Oct) 1167–1174.
[30] R.J. Shaw, K.A. Lamia, D. Vasquez, et al., The kinase LKB1 mediates glucose homeostasis in liver and therapeutic effects of metformin, Science 310 (2005) 1642–1646.
[31] M.R. Owen, E. Doran, A.P. Halestrap, Evidence that metformin exerts its anti-diabetic effects through inhibition of Complex 1 of the mitochondrial respiratory chain, Biochem J 348 (2000) 607–614.
[32] B. Viollet, B. Guigas, N. Sanz Garcia, J. Leclerc, M. Foretz, F. Andreelli, Cellular and molecular mechanisms of metformin: an overview, Clin Sci 122 (2012) 253–270.
[33] H. Mashhedi, M.J. Blouin, M. Zakikhani, et al., Metformin abolishes increased tumor (18)F-2-fluoro-2-deoxy-D-glucose uptake associated with a high energy diet, Cell Cycle 10 (2011) 2770–2778.
[34] M. Foretz, B. Guigas, L. Bertrand, M. Pollak, B. Viollet, Metformin: from mechanisms of action to therapies, Cell Metab 20 (2014) 953–966.
[35] M. Massollo, C. Marini, M. Brignone, et al., Metformin temporal and localized effects on gut glucose metabolism assessed using 18F-FDG PET in mice, J Nucl Med 54 (2013) 259–266.
[36] M.N. Pollak, Investigating metformin for cancer prevention and treatment: the end of the beginning, Cancer Discov 2 (9) (2012) 778–790.
[37] C.S. Patlak, R.G. Blasberg, J.D. Fenstermacher, Graphical evaluation of blood-to-brain transfer constants from multiple-time uptake data, J Cereb Blood Flow Metab 3 (1983) 1–7.
[38] M. Scussolini, M. Bauckneht, V. Cossu, et al., G6Pase location in the endoplasmic reticulum: implications on compartmental analysis of FDG uptake in cancer cells, Sci Rep 9 (1) (2019) 2794.
[39] B.N. Zordoky, D. Bark, C.L. Soltys, M.M. Sung, J.R.B. Dyck, The anti-proliferative effect of metformin in triple-negative MDA-MB-231 breast cancer cells is highly dependent on glucose concentration: implications for cancer therapy and prevention, Biochim Biophys Acta 1840 (6) (2014) 1943–1957.
[40] Y. Zhuang, W.K. Miskimins, Cell cycle arrest in metformin treated breast cancer cells involves activation of AMPK, downregulation of cyclin D1, and requires p27Kip1 or p21Cip1, J Mol Signal 3 (2008) 18.
[41] K. Green, M.D. Brand, M.P. Murphy, Prevention of mitochondrial oxidative damage as a therapeutic strategy in diabetes, Diabetes 53 (Suppl. 1) (2004) S110–S118.
[42] J.L. Evans, I.D. Goldfine, B.A. Maddux, G.M. Grodsky, Oxidative stress and stress-activated signaling pathways: a unifying hypothesis of type 2 diabetes, Endocr Rev 23 (2002) 599–622.
[43] D.K. Zaafar, S.A. Zaitone, Y.M. Moustafa, Role of metformin in suppressing 1,2 dimethylhydrazine-induced colon cancer in diabetic and non-diabetic mice: effect on tumor angiogenesis and cell proliferation, PLoS One 9 (2014), e100562.
[44] K. Srinivasan, B. Viswanad, L. Asrat, C.L. Kaul, P. Ramarao, Combination of high-fat diet-fed and low-dose streptozotocin-treated rat: A model for type 2 diabetes and pharmacological screening, Pharmacol Res 52 (2005) 313–320.
[45] J.F. Aileen, King. The use of animal models in diabetes research, Br J Pharmacol 166 (3) (2012) 877–894.
[46] D. Zechner, T. Radecke, J. Amme, et al., Impact of diabetes type II and chronic inflammation on pancreatic cancer, BMC Cancer 15 (2015) 51.